

Article

Exploring the Viability of Utilizing Treated Wastewater as a Sustainable Water Resource for Green Hydrogen Generation Using Solid Oxide Electrolysis Cells (SOECs)

Marina Maddaloni ^{1,2,3}, Matteo Marchionni ⁴, Alessandro Abbá ², Michele Mascia ⁴, Vittorio Tola ⁴, Maria Paola Carpanese ⁵, Giorgio Bertanza ² and Nancy Artioli ^{1,2,*}

- ¹ CEEP Laboratory, Department of Civil Engineering, Architecture, Territory, Environment and Mathematics, University of Brescia, via Branze 38, 25123 Brescia, Italy; marina.maddaloni@unibs.it
- ² Department of Civil, Environmental, Architectural Engineering and Mathematics, University of Brescia, via Branze, 43, 25123 Brescia, Italy; alessandro.abba@unibs.it (A.A.); giorgio.bertanza@unibs.it (G.B.)
- ³ Consorzio Interuniversitario Nazionale per la Scienza e Tecnologia dei Materiali (INSTM), University of Brescia, via Branze 38, 25123 Brescia, Italy
- ⁴ Department of Mechanical, Chemical and Materials Engineering, University of Cagliari, via Marengo 2, 09123 Cagliari, Italy; matteo.marchionni@unica.it (M.M.); michele.mascia@unica.it (M.M.); vittorio.tola@unica.it (V.T.)
- ⁵ Department of Civil, Chemical and Environmental Engineering, University of Genova (UNIGE-DICCA), via Montallegro 1, 16145 Genoa, Italy; maria.paola.carpanese@unige.it
- * Correspondence: nancy.artioli@unibs.it

Abstract: In response to the European Union's initiative toward achieving carbon neutrality, the utilization of water electrolysis for hydrogen production has emerged as a promising avenue for decarbonizing current energy systems. Among the various approaches, Solid Oxide Electrolysis Cell (SOEC) presents an attractive solution, especially due to its potential to utilize impure water sources. This study focuses on modeling a SOEC supplied with four distinct streams of treated municipal wastewaters, using the Aspen Plus software. Through the simulation analysis, it was determined that two of the wastewater streams could be effectively evaporated and treated within the cell, without generating waste liquids containing excessive pollutant concentrations. Specifically, by evaporating 27% of the first current and 10% of the second, it was estimated that 26.2 kg/m³ and 9.7 kg/m³ of green hydrogen could be produced, respectively. Considering the EU's target for Italy is to have 5 GW of installed power capacity by 2030 and the mass flowrate of the analyzed wastewater streams, this hydrogen production could meet anywhere from 0.4% to 20% of Italy's projected electricity demand.

Keywords: green hydrogen; wastewater; renewable energy sources



Citation: Maddaloni, M.; Marchionni, M.; Abbá, A.; Mascia, M.; Tola, V.; Carpanese, M.P.; Bertanza, G.; Artioli, N. Exploring the Viability of Utilizing Treated Wastewater as a Sustainable Water Resource for Green Hydrogen Generation Using Solid Oxide Electrolysis Cells (SOECs). *Water* **2023**, *15*, 2569. <https://doi.org/10.3390/w15142569>

Academic Editor: William Frederick Ritter

Received: 20 June 2023
Revised: 9 July 2023
Accepted: 11 July 2023
Published: 13 July 2023



Copyright: © 2023 by the authors. Licensee MDPI, Basel, Switzerland. This article is an open access article distributed under the terms and conditions of the Creative Commons Attribution (CC BY) license (<https://creativecommons.org/licenses/by/4.0/>).

1. Introduction

The European Union is taking on climate change through an ambitious energy transition program to achieve carbon neutrality by 2050. The aim is to reduce emissions by over 85% by adopting Renewable Energy Sources (RESs) [1].

By transitioning to RESs, the aim is to decrease the current heavy dependence on fossil fuels and energy imports by over 70%, thereby benefiting the environment and the economy. This includes adopting sustainable heating in buildings through RESs like electro-fuels, green H₂, and biogas [2–4].

In the transportation sector, the automotive industry is investing in low-emission technologies such as electric vehicles [5,6]. However, current batteries do not meet the requirements for long-haul transport, limiting their use in areas like air and maritime transportation [7–10].

To address this challenge, biofuels offer a promising option for achieving substantial emission reduction [11,12]. Within this context, H₂-based technologies can play a crucial

role as medium- and long-term solutions [13]. However, transitioning to a hydrogen-based economy, alongside the electrification of a growing share of the energy sector and the utilization of bio-based carbon sources, may not be sufficient to attain carbon neutrality. Many industrial processes use fossil sources as carbon feedstocks and release significant CO₂ emissions that are challenging to mitigate. Consequently, alongside emission reduction efforts [14–16], it becomes necessary to capture, store, and utilize emitted CO₂.

The development of technologies for Carbon Capture and Utilization (CCU) will play an increasingly vital role in this endeavor. Among these technologies, Power-to-X (P2X) approaches have emerged as prominent methods to convert electrical energy into synthetic liquids or gases (such as hydrogen, methanol, and methane) [17–19], utilizing captured CO₂ as a feedstock. Notably, the Power-to-Methanol technology stands out as it captures CO₂ emissions, combines CO₂ with H₂ to produce methanol, and reintroduces them into industrial processes as a renewable energy source, aligning with the principles of a circular economy [20–23].

To achieve the widespread adoption of green hydrogen as part of the global energy transition, electrolysis has emerged as a key process for hydrogen production, which utilizes only water and electricity, with the sole by-product being oxygen according to the reaction shown in Equation (1) [24]:



The two well-established low-temperature processes, alkaline and Polymer Electrolyte Membrane (PEM) electrolysis, are the main industrial electrolysis processes. An alkaline electrolyzer (AE) generally uses nickel-based electrodes, porous separators such as Zirfon® from Agfa which is composed of a polysulfone matrix and ZrO₂ powder [25], and concentrated KOH solution as the electrolyte. A cell of this type generally operates under mild conditions, with temperatures in the range between 30 and 80 °C and current densities below 1 A cm⁻². Anion-Exchange Membranes (AEMs) are expected to replace separators, thus increasing the performance to values similar to PEM electrolyzers [26]. A PEM electrolyzer also works in the temperature range between 20 and 80 °C. Its high activity in the production of H₂ from water is ensured by the high current densities (well above 1 A cm⁻²), but PEM uses noble metals at the cathode (generally Pt/Pd) and at the anode (usually constituted by IrO₂/RuO₂) [27]. Both technologies produce hydrogen at low temperatures, with relatively high energy demands. Both PEM electrolysis and AEM electrolysis operate at cold startup times with very low temperatures and could be effectively powered with renewable energy sources for storage or use in transport applications.

However, high-temperature processes can be exploited to supply green hydrogen, including methanol synthesis, allowing the thermal integration between electrolyzers and reactors [28].

Solid Oxide Electrolysis Cells (SOECs) are electrolytic cells capable of operating in harsh conditions of high pressure and high temperature until reaching a range between 500 and 850 °C. This allows the use of incoming water in the gaseous form [29]. The structure of these cells is characterized by a solid cathode and a solid anode, which are separated by a solid porous electrolyte that is capable of conducting O²⁻ ions generated at the cathode [28]. The most commonly used electrolytes are yttria–zirconia-based materials (YSZ) due to their high stability, low toxicity, and high abundance [30,31], but in recent years, electrolytes based on ceria, such as Gadolinium-Doped Ceria (GDC) or Samarium-Doped Ceria (SDC), are replacing conventional YSZ electrolytes due to their higher conductivity [32]. Recently, these materials have also been often employed as cathodes as an alternative to the most common Ni-cements, especially in the case of cells with YSZ electrolytes [33], for which they show good compatibility. In an SOEC, the O²⁻ ions generated at the cathode and transported by the electrolyte are used at the anode to form O₂(g) and electrons; thus, a good anode for these cells must be characterized by high ionic and electronic conductivities.

Perovskites and perovskite-based materials have been proven to be particularly suitable for the role [28].

Both PEMs and AEs require a high purity of the inlet water to produce hydrogen [27], and this could be a problem since fresh water is a scarce and precious resource that is destined to become even more scarce due to the increase in world population, global warming, and widespread pollution of water bodies [2,34,35]. For this reason, it is essential to study alternatives that allow the exploitation of the abundance of different high-salinity concentrated seawaters, rainwaters, and industrial or urban wastewaters, thereby keeping a high efficiency in water conversion.

In this context, SOECs could represent a concrete possibility to spread the use of Power-to-Methanol technologies on a global scale for the production of green hydrogen, but without tapping into clean water sources that are already rare on the planet. Moreover, their high efficiency (~90–100%), the possibility to use high pressure, and the high purity of the obtained hydrogen make these electrolytic cells competitive both in PEMs and AEs for industrial purposes [36,37].

The main advantage of SOECs is that this type of high-temperature electrolyzers uses evaporated water flows and, therefore, unlike AEs and PEMs, pure water is not required. In fact, if wastewater is evaporated, the impurities and salts present in the starting batch can be mostly separated from the inlet vapor, thereby avoiding adverse effects on solid oxide electrolysis cells but still using wastewater without further treatment. This is a fundamental aspect because it opens the door to the use of impure water to obtain high-quality level of green hydrogen, not only in highly industrialized areas, where industrial wastewaters can be used by maintaining the principles of a circular economy, but also in areas of the world where clean water is scarce even for the needs of the population.

However, at present, SOECs are still in an experimental phase, and despite the availability of some studies on the use of these cells to directly split seawater [35,37–40], there is no application that involves the use of wastewater. There are two main concerns about direct wastewater electrolysis in SOECs: (i) the value of energy consumption due to a possible wastewater pre-treatment and its evaporation, and (ii) the heterogenic composition of wastewater.

In particular, the management of municipal and industrial wastewaters is described in Figure 1. Industrial wastewater can be discharged into the environment (such as surface water) after its treatment in a complete industrial WasteWater Treatment Plant (WWTP); alternatively, and most commonly, as shown in Figure 1, it can be pre-treated in an industrial WWTP and discharged in a public sewer (for this, specific standards must be complied with the Limit PS), together with domestic wastewater. This means that urban wastewater (the mixture of industrial and domestic flows) quality could also vary according to the percentage and type of industrial wastewater [41]. In Italy, treated municipal wastewater to be discharged into surface water must comply with the limits imposed by the country, or with more restrictive limits provided by regional regulations (Limit SW) [42,43].

The novelty of this study lies in its emphasis on the potential of SOECs that could operate effectively using treated wastewaters as the water sources by exploiting the possibility of operating in high-temperature conditions and using water in its gas form as the inlet source. In pursuit of this objective, the focus begins with real wastewaters that have undergone treatment in a municipal wastewater treatment plant (represented as streams A, B, C, and D in Figure 1). To assess the energy balance of the system under investigation, detailed models of the main sections of the SOEC plant, which receives steam from wastewater, were developed and implemented using the commercial software Aspen Plus by AspenTech. These models were employed to analyze and evaluate the energy requirements and overall efficiency of the proposed system.

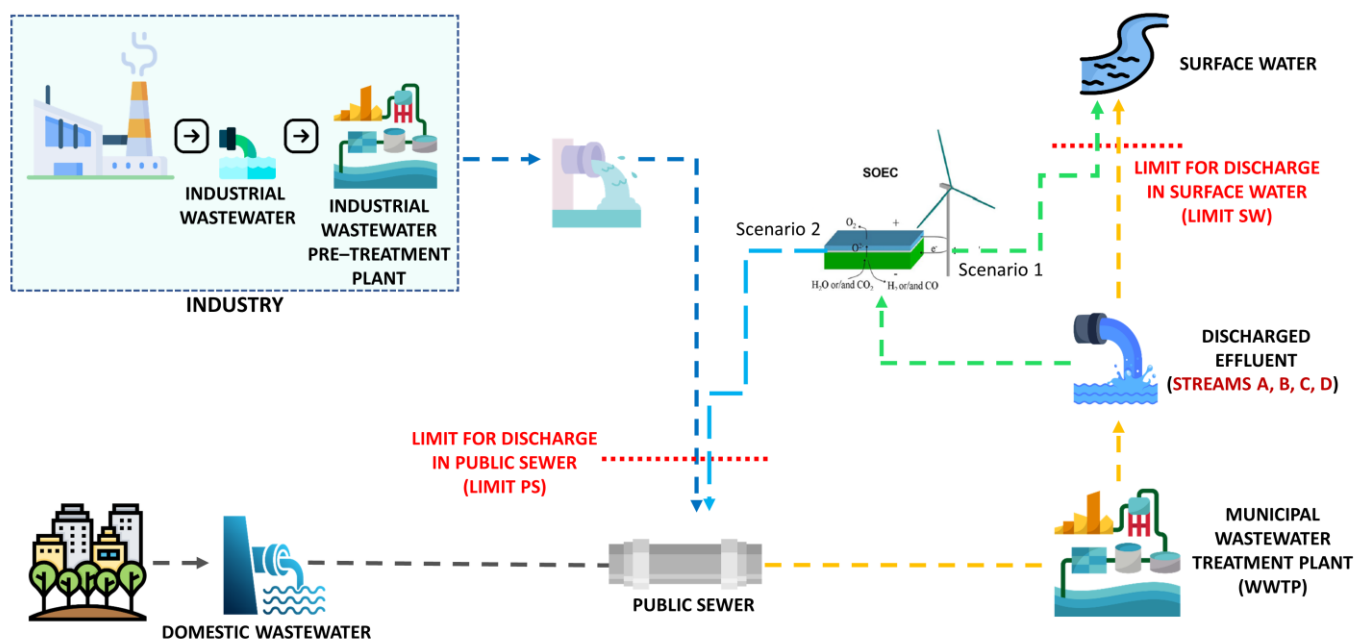


Figure 1. Schematic representation of the destiny of domestic and industrial wastewaters. Industrial wastewater can be discharged in public sewers if it respects the limits reported in the Materials and Methods section (Limit PS). Urban wastewaters (industrial + domestic wastewaters) conveyed by public sewers are sent to a municipal wastewater treatment plant (WWTP). The treated wastewater (streams A, B, C, and D) can be discharged into surface water if they respect the Limit SW, or they can be sent to a SOEC for the conversion of H₂O into H₂. The liquid that remains after the evaporation of the streams can be discharged into surface water (Scenario 1) if it respects the Limit SW or, if it does not, it can be re-discharged into public sewers for another cycle (Scenario 2).

2. Materials and Methods

2.1. Treated Wastewater Stream Description

Four different treated wastewaters were selected for the purpose of this study. These wastewaters, referred to as streams A, B, C, and D, originated from four municipal wastewater treatment plants (WWTPs) located in Northern Italy. Each stream had distinct characteristics in terms of capacity (expressed as population equivalent, P.E.), industrial load, and treatment scheme. The main features of these WWTPs are provided in Table 1.

Table 1. Main features of the analyzed WWTPs.

	WWTP A	WWTP B	WWTP C	WWTP D
Capacity [P.E.]	620,600	160,000	120,500	52,000
Average flow rate [m ³ /d]	155,300	50,400	27,500	23,300
Industrial load [%]	15	19	11	25
WWTP scheme	Activated sludge with pre- and post-denitrification; tertiary filtration	Membrane bioreactor (MBR) with pre-denitrification	Activated sludge with alternating oxic/anoxic cycles; tertiary filtration	Activated sludge; tertiary filtration

The compositions of the four wastewater streams are shown in Table 2. The values presented in the table represent the average measurements obtained from the samples collected over a one-year period (2022), with a minimum sampling frequency of once per month. The gas chromatography/mass spectrometry (GC/MS) analyses revealed that the main components contributing to the chemical oxygen demand (COD) include proteins (17%), volatile fatty acids (13%), and sugars (20%). The remaining 50% consists of high-molecular-weight soluble organics, such as humic acids and nucleic acids.

Table 2. Description of the compositions of the four real treated wastewater streams under cons. n.a.: not available; n = number of data; E.C.: electrical conductivity at 25 °C; COD: chemical oxygen demand; BOD₅: biological oxygen demand at 5 days; TSS: total suspended solid; TN: total nitrogen; TP: total phosphorus; HCs: hydrocarbons; CFU: Colony-Forming Units.

Composition		STREAM A (n = 54)		STREAM B (n = 75)		STREAM C (n = 54)		STREAM D (n = 61)	
		Average	95th Percentile						
pH	[-]	7.6	7.7	7.7	8.0	7.6	7.8	7.6	7.9
E.C.	[µS/cm]	780	889	637	788.8	606	741	672.1	874.2
COD	[mg/L]	19	22	15.2	15	15.3	16.8	15.5	18
BOD ₅	[mg/L]	5.4	7	5.4	9.3	5.7	9.0	5.5	8.0
TSS	[mg/L]	6.6	5.0	6.4	9.3	5.7	8.8	5.7	11
TN	[mg/L]	7.3	9.6	6.4	10.3	3.9	6.8	9.0	19
TP	[mg/L]	0.7	1.0	0.9	1.5	0.7	1.0	0.5	0.8
Al	[mg/L]	0.20	0.25	0.11	0.20	0.1	0.1	0.1	0.1
As	[mg/L]	0.03	0.03	0.014	0.030	0.02	0.03	0.018	0.030
Ba	[mg/L]	n.a.	n.a.	0.1	0.1	n.a.	n.a.	0.1	0.1
Bo	[mg/L]	n.a.	n.a.	0.11	0.17	n.a.	n.a.	0.22	0.63
Cd	[mg/L]	0.01	0.01	0.003	0.010	0.005	0.01	0.005	0.01
Cr _{TOT}	[mg/L]	0.1	0.1	0.033	0.1	0.05	0.1	0.045	0.100
Cr(VI)	[mg/L]	n.a.	n.a.	n.a.	n.a.	n.a.	n.a.	n.a.	n.a.
Fe	[mg/L]	0.12	0.25	0.2	0.4	0.1	0.1	0.098	0.100
Mn	[mg/L]	0.17	0.20	0.20	0.10	0.06	0.10	0.063	0.100
Hg	[mg/L]	n.a.	n.a.	0.0005	0.0005	n.a.	n.a.	0.005	0.005
Ni	[mg/L]	0.1	0.1	0.036	0.10	0.05	0.1	0.046	0.100
Pb	[mg/L]	0.1	0.1	0.051	0.100	0.07	0.1	0.058	0.100
Cu	[mg/L]	0.013	0.025	0.011	0.020	0.013	0.026	0.010	0.010
Zn	[mg/L]	0.08	0.24	0.11	0.28	0.09	0.11	0.08	0.13
Chloride (Cl ⁻)	[mg/L]	100.7	121.1	59.0	89.2	48.4	76.2	60.2	102.4
Sulphate (SO ₄ ²⁻)	[mg/L]	51	54	38.4	52.1	27	38	37.4	43.0
Sulphite (SO ₃ ⁻)	[mg/L]	n.a.	n.a.	0.2	0.2	n.a.	n.a.	0.5	0.5
Sulphide (S ²⁻)	[mg/L]	n.a.	n.a.	0.1	0.1	n.a.	n.a.	0.1	0.1
Cyanide (CN ⁻)	[mg/L]	n.a.	n.a.	0.01	0.01	n.a.	n.a.	0.01	0.01
Fluoride (F ⁻)	[mg/L]	n.a.	n.a.	0.25	0.25	n.a.	n.a.	0.25	0.25
Phenols	[mg/L]	n.a.	n.a.	0.1	0.1	n.a.	n.a.	0.1	0.1
Total HCs	[mg/L]	n.a.	n.a.	0.05	0.05	n.a.	n.a.	0.5	0.5

2.2. Balance of the Plant for H₂ Production through Electrolysis

The balance of the plant (BOP) for the wastewater-feed SOEC electrolyzer was performed using the Aspen Plus software (AspenTech). The first unit in the process is the evaporator/steam generator, which generates the SOEC feed from the wastewaters. The evaporator produces two streams: a concentrated liquid stream and a vapor stream. The pollutant concentration of the liquid stream after evaporation was determined through mass balances as follows:

$$Wx_W = Lx_L \quad (2)$$

$$W = L + V \quad (3)$$

where W and x_W are the flow rate and concentration of pollutants in the wastewater, L and x_L the corresponding values in the liquid outlet, and V is the flow rate of vapor. The vapor fraction was calculated as follows:

$$V_{\%} = \frac{V}{W} = \left(1 - \frac{x_W}{x_L}\right) \quad (4)$$

To simulate the organic content of wastewaters, key components were used for representation in the simulation. Glutamine, glucose, and acetic acid were selected to represent the three main fractions of the organic content. Curcumin was chosen as the key component to represent the remaining organic load. These components were utilized in the simulation for accurate representation and analysis of wastewater composition.

2.3. SOEC

2.3.1. System Description

SOEC-based electrolyzers offer the advantages of reduction in electricity consumption required for water splitting and hydrogen production by utilizing thermal energy. Unlike low-temperature electrolyzers, a portion of the energy is supplied as heat in the high-temperature reaction, which is achieved by vaporizing and heating the water and air used in the process.

Figure 2 illustrates the scheme of the electrolysis stack. The wastewater feed is divided into two sub-streams, with one sub-stream facilitating the recovery of residual heat from the cell products, thereby minimizing the thermal input needed from external energy sources.

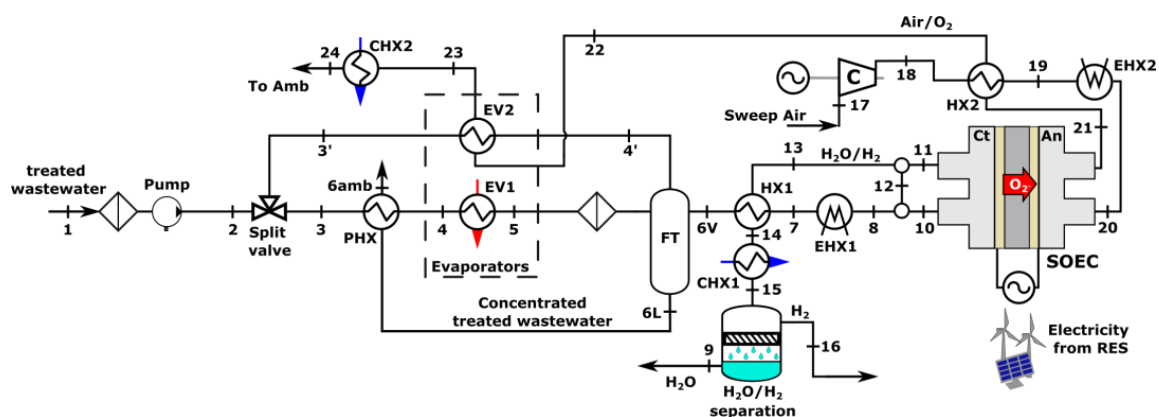


Figure 2. Layout of the SOEC stack, where numbers identify the several streams in the layout whose temperature and mass flow are reported in Table 4.

Both sub-streams (node 3 and node 3') undergo vaporization in the evaporators EV1 and EV2, respectively, until reaching the maximum allowable concentration limits of pollutants in the residual liquid. In the flash tank (FT), the saturated steam is separated from the more concentrated wastewater, which remains in a saturated liquid state before being

discharged into surface water. The concentrated wastewater (node 6L) is used to pre-heat the first sub-stream in the heat exchanger PHX before being released into the environment.

The saturated stream (node 6V) is then heated in the heat exchanger HX1 using the residual heat from the cathodic exhaust gases (a mixture of hydrogen and steam) exiting the electrolyzer (node 13). Subsequently, the stream is further heated to the operating temperature of the SOEC using the electric heater EHX1 and combined with a mixture of hydrogen and steam (10%/90% composition, node 12) to prevent electrode oxidation. After cooling in the heat exchangers HX1 and CHX1, the hydrogen and water mixture is separated, with the condensed water carrying only a fraction of the pollutants present in the original stream. This condensed water can undergo moderate chemical treatment processes and be utilized for domestic or industrial applications.

In the SOEC, oxygen produced during the electrolysis reaction passes through the SOEC membrane and is removed from the anode using a sweep gas stream (in this case, air). Air is heated to the cell's operating temperature in the heat exchanger HX2 and the electric heater EHX2. The residual heat from the anodic exhausts (a mixture of air and oxygen) is used to heat the incoming air stream downstream of the compressor C and to vaporize the second sub-stream of wastewater in the evaporator EV2 before being released into the environment.

2.3.2. Modeling Approach

The stack model was incorporated into Aspen Plus [44], utilizing an electrochemical model for the cell based on the approach described in [45–47]. This model is specifically designed for planar cells. The calculation of the cell voltage is determined based on Equation (5), taking into account various factors. The overpotential caused by the ohmic resistance in the cell is represented by η_{ohm} , while η_{act} and η_{conc} correspond to the activation and concentration overpotentials at both the anode and the cathode. These overpotentials are influenced by the reaction kinetics and electrode geometry [45,48].

$$E_{SOEC} = E_{eq} + (\eta_{ohm} + (\eta_{act} + \eta_{conc})_{an} + (\eta_{act} + \eta_{conc})_{cat}) \quad (5)$$

The cell potential, E_{eq} , is determined using the Nernst equation, as shown in Equation (6). The reversible voltage, E_0 , is a function of the operating temperature of the cell, T_c , as defined in Equation (7) [49]. In these equations, F represents the Faraday constant, R is the gas constant, and p_i denotes the partial pressure of the i -th chemical species involved in the cell's reaction.

$$E_{eq} = E_0 + \frac{RT_c}{2F} \ln\left(\frac{p_{H_2} p_{O_2}}{p_{H_2O}}\right) \quad (6)$$

$$E_0 = 1.253 - 2.4516 \times 10^{-4} T_c \quad (7)$$

The electric power consumption of the electrolyzer, denoted as P_{SOEC} , can be determined using Equation (8). In this equation, J represents the cell current density, and A corresponds to the electrode area of the planar cell:

$$P_{SOEC} = E_{SOEC} J A \quad (8)$$

The efficiency of the SOEC can be calculated using Equation (9), where $P_{el,EHX}$ represents the electrical power supplied to the electric heaters:

$$\eta_{SOEC} = \frac{\dot{m}_{H_2} LHV_{H_2}}{P_{SOEC} + P_{el,EHX}} \quad (9)$$

The thermal model incorporates the energy and mass balance equations for the heat exchangers, valves, and split junctions, as shown in Equations (10) and (11):

$$\dot{m}_{in} = \dot{m}_{out} \tag{10}$$

$$\dot{m}_{cs}(h_{in} - h_{out}) = \dot{m}_{hs}(h_{in} - h_{out}) \tag{11}$$

where *cs* and *hs* stand for the cold side and the hot side, respectively, while *in* and *out* stand for the inlet and the outlet

The equations assume negligible pressure drops along the heat exchangers, pipes, valves, split junctions, as well as within the cell electrodes. Thermal losses to the environment are also disregarded, considering the system as being insulated. Additionally, the calculations do not consider the thermal inertia of metals and materials, employing a lumped modeling approach. For a comprehensive understanding of the SOEC model, see [50].

3. Results and Discussions

As mentioned earlier, depending on the situation considered, the reference concentrations of pollutants in the liquid streams can be either those meeting the requirements for discharge into surface water (Limit SW) or, alternatively, into public sewers (Limit PS). The potential vapor flow rate that can be obtained from each wastewater stream was calculated using Equation (2), with *xL* representing the limits specified in Table 3.

Table 3. Composition of the treated wastewaters considered (original liquid stream), and maximum evaporation percentage to fulfil the limits for surface water (Scenario 1) and public sewers (Scenario 2). The components that limit evaporation are in red. n.a.: not available.

	Original Liquid Stream (mg/L)				Scenario 1					Scenario 2				
	A	B	C	D	V (%)				Limits SW (mg/L)	V (%)				Limits PS (mg/L)
					ASW	BSW	CSW	DSW		APS	BPS	CPS	DPS	
COD	22	15	16.8	18	63.3	75	72	70	60	95.8	97	96.6	96.4	500
BOD ₅	7	9.3	9	8	30	7	10	20	10	97.2	96.3	96.4	96.8	250
TSS	5	9.3	8.8	11	66.7	38	41.3	26.7	15	97.5	95.4	95.6	94.5	200
TN	7.3	6.4	3.9	9	27	36	61	10	10	86.5	88.1	92.8	83.3	53.9
TP	0.7	0.9	0.7	0.5	30	10	30	50	1	93	91	93	95	10
Al	0.245	0.2	0.1	0.1	75.5	80	90	90	1	87.8	90	95	95	2
As	0.03	0.003	0.03	0.03	94	94	94	94	0.5	94	94	94	94	0.5
Ba	n.a.	0.1	n.a.	0.1	-	99.5	-	99.5	20	-	-	-	-	1000
Bo	n.a.	0.17	n.a.	0.63	-	91.5	-	68.5	2	-	95.8	-	84.3	4
Cd	0.01	0.01	0.01	0.01	50	50	50	50	0.02	50	50	50	50	0.02
Fe	0.25	0.4	0.1	0.1	87.5	80	95	95	2	93.8	90	97.5	97.5	4
Mn	0.2	0.1	0.1	0.1	90	95	95	95	2	95	97.5	97.5	97.5	4
Ni	0.1	0.1	0.1	0.1	95	95	95	95	2	97.5	97.5	97.5	97.5	4
Pb	0.1	0.1	0.1	0.1	50	50	50	50	0.2	66.7	66.7	66.7	66.7	0.3
Cu	0.025	0.02	0.025	0.01	75	80	75	90	0.1	93.8	95	93.8	97.5	0.4
Zn	0.24	0.28	0.11	0.13	52	44	78	74	0.5	76	72	89	87	1
Hg	n.a.	0.0005	n.a.	0.005	-	90	-	0	0.005	-	90	-	0	0.005

Table 3 displays the values of V: the minimum value in each column indicates the maximum percentage of vapor that can be generated from each stream. Higher evaporation would result in at least one concentration value exceeding the relevant limits set by Italy’s national (Legislative Decree No. 152/2006 and subsequent modifications, known as the “Environmental Code”) [51] and Lombardy’s (Regional Regulation No. 6/2019) regulations [52].

In the “Scenario 1” section of the table, the maximum evaporation percentages for each stream (ASW, BSW, CSW, and DSW) are provided to achieve a residual liquid fraction

in which the concentration of each component adheres to the limits specified for discharge into surface water (Limits SW). In the “Scenario 2” section, the maximum evaporation percentages for each stream (APS, BPS, CPS, and DPS) are given to obtain a residual liquid where the concentration of each component meets the limits set for discharge into public sewers (Limits PS).

As shown in Table 3, the concentration values in Scenario 2 do not significantly limit the vapor fraction since the minimum value of 50% (set to match the limit of Cd) is relatively high for most industrial steam generators and reboilers. However, the limits of Scenario 2 will not be considered in the simulations because the outlet stream from the SOEC should be recycled back to the wastewater treatment plant (WWTP) for further processing before being discharged into surface water, in accordance with the information provided in Figure 1.

Based on the values in Scenario 1, stream D cannot be considered due to one parameter (specifically Hg) reaching the relevant limit. Streams B and C could provide similar percentages of steam, but only stream C was selected for further analysis. The energy analysis was subsequently conducted using streams A and C.

SOEC Simulation

The electrochemical model of the SOEC electrolyzer underwent validation using experimental data from the literature [47]. Figure 3 illustrates the results of this validation process. The continuous lines in the figure represent the relationship between cell potential and the electrolyzer’s current density, while varying the operating temperature of the stack. The cell’s operating temperature range is from 900 °C to 1000 °C. The experimental data points are depicted using different symbols corresponding to the respective operating temperatures. The simulation results demonstrate a favorable agreement with the experimental data, with an absolute maximum error of only 2.7%. The experimental study involved potential and frequency measurements conducted with an accuracy of 1 μ V and 0.1°, respectively [53]. Overall, the model effectively replicates the behavior and performance of the SOEC as observed in the experimental observations. It also indicates a linear proportional trend that closely approximates the relationship between current density and cell potential, with the slope being dependent on the cell’s operating temperature.

In this study, the validated model was employed to evaluate the hydrogen production and performance of the electrolyzer using different wastewater streams. Among the considered streams (A, B, and C), only three met the concentration limits for pollutants, making them suitable for supplying the electrolyzer. Stream B, however, was excluded due to its low vaporization rate of 7%, which would result in concentrations of pollutants exceeding the allowable limits, as shown in Table 3.

The simulation results, presented in Table 4, provide insights into the temperature levels, phase states, and fluid qualities within the stack (referencing node numbers in Figure 2). To minimize heat consumption, each wastewater stream is divided into sub-streams within the electrolyzer. Table 4 also presents the relative mass flow rates at different nodes of the stack, which were calculated as the ratio of the fluid’s mass flow rate at a specific node to the nominal mass flow rate of wastewater processed in the electrolyzer.

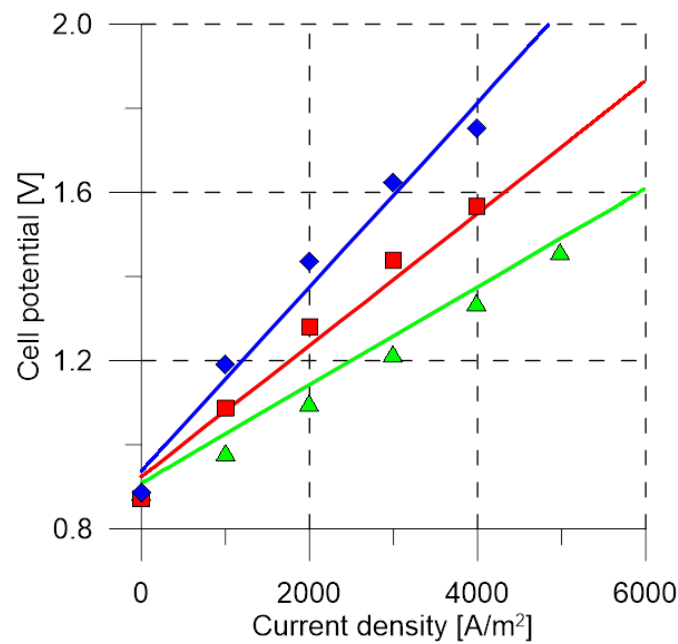


Figure 3. Model validation using experimental (exp) data reported in [47].

For comparison purposes, an equal nominal mass flow rate of wastewater was set for both streams. To minimize the thermal input required from external energy sources, a mass flow rate split ratio of four was chosen, as determined by dividing the mass flow rate of the sub-stream at node 3 by the mass flow rate of the sub-stream at node 3' (Figure 2). This optimized split ratio helps to achieve efficient operation while maintaining hydrogen production.

Overall, the utilization of the validated model allows us to analyze the hydrogen production potential and assess the performance of the electrolyzer when operating with different wastewater streams. The results highlight the importance of selecting appropriate streams that comply with concentration limits and optimizing the mass flow rate split ratio to minimize energy consumption during the electrolysis process.

By analyzing the values presented in Table 4, we observe that although the temperature levels across the stack remain the same in both cases, there are differences in the relative mass flow rate and water stream quality due to the distinct vaporization rates permitted for stream A (27%) and stream C (10%). The operating temperature of the SOEC was set at 839 °C, enabling thermoneutral voltage operation. This condition enhances efficiency as the cell can operate without any thermal energy inflow or outflow, thus simplifying the stack operation and thermal management [54].

The performance of the SOEC per kilogram of hydrogen produced is summarized in Table 5. The electric energy required to split water at a high temperature is 34.3 kWh/kgH₂, with an additional 1.3 kWh/kgH₂ needed to heat up water vapor from 673 °C to 839 °C and air stream from 789 °C to 839 °C using the electric heaters (EHX1 and EHX2 in Figure 2). In general, the total heat consumption of the cell is 14.6 kWh/kgH₂, of which 6.4 kWh/kgH₂ is provided by external sources (including 1.3 kWh/kgH₂ through the electric heaters), and 8.2 kWh/kgH₂ is recovered from the residual heat of the anodic and cathodic exhausts. This recovery accounts for 56% of the total consumption, thus enhancing the efficiency of the electrolyzer.

Table 4. Results of the simulations performed using the Aspen model of the SOEC and considering two treated wastewater streams, A and C (nodes refer to Figure 2). Temperature levels, mass flow rates (MFR), phase and quality of the different sub-streams are reported. When water is in two-phase (TP) conditions, the quality column indicates the mass percentage of vapor present in the mixture. Otherwise, the notations, sub-cooled (SC) and super-heated (SH), are used to indicate that water is in an unsaturated liquid or vapor conditions, respectively. At node 15, the notation, mixed (M), is used to indicate the presence of water in the liquid (L) phase and hydrogen in the gaseous (G) phase.

Node	STREAM A				STREAM C			
	Temperature [°C]	MFR	Phase	Quality	Temperature [°C]	MFR	Phase	Quality
Wastewater								
1	25	1.000	L	SC	25	1.000	L	SC
2	25	1.000	L	SC	25	1.000	L	SC
3	25	0.800	L	SC	25	0.800	L	SC
3'	25	0.200	L	SC	25	0.200	L	SC
4	72	0.800	L	SC	72	0.800	L	SC
4'	100	0.200	TP	0.27	100	0.200	TP	0.10
5	100	0.800	TP	0.27	100	0.800	TP	0.10
6 L	100	0.730	L	0	100	0.900	L	0
6 amb	35	0.730	L	SC	35	0.900	L	SC
Water								
6 V	100	0.270	G	1	100	0.100	G	1
7	673	0.270	G	SH	673	0.100	G	SH
8	839	0.270	G	SH	839	0.100	G	SH
9	25	0.040	L	SC	25	0.013	L	SC
Water/Hydrogen								
10	839	0.276	G	SH	839	0.103	G	SH
11	839	0.070	G	SH	839	0.026	G	SH
12	839	0.005	G	SH	839	0.003	G	SH
13	839	0.065	G	SH	839	0.023	G	SH
14	150	0.065	G	SH	150	0.023	G	SH
15	25	0.065	M	SC/SH	25	0.023	M	SC/SH
Hydrogen								
16	25	0.026	G	SH	25	0.010	G	SH
Air								
17	25	0.292	G	SH	25	0.109	G	SH
18	25	0.292	G	SH	25	0.109	G	SH
19	789	0.292	G	SH	789	0.109	G	SH
20	839	0.292	G	SH	839	0.109	G	SH
Air/Oxygen								
21	839	0.503	G	SH	839	0.186	G	SH
22	400	0.503	G	SH	400	0.186	G	SH
23	79	0.503	G	SH	79	0.186	G	SH
24	25	0.503	G	SH	25	0.186	G	SH

Table 5. SOEC performance and consumption per kg of hydrogen produced.

	Unit	Value
Electricity	[kWh/kgH ₂]	34.5
Heat duty	[kWh/kgH ₂]	14.6
Heat recovered	[kWh/ kgH ₂]	8.2
Heat from external sources	[kWh/ kgH ₂]	6.4
Heat share recovered	[%]	56
SOEC efficiency	[%]	85

The efficiency of the SOEC, as detailed in Equation (9), was calculated by dividing the chemical energy of hydrogen produced from the wastewater stream by the electricity consumption required to produce it. The obtained value of 85% indicates that 15% of

energy consumption is lost during the hydrogen production process. This value aligns with the efficiency values of SOEC cells reported in the literature [46] and exceeds those of low-temperature PEM and alkaline electrolyzers due to the higher temperature at which the water splitting reaction occurs.

Table 6 presents the values of hydrogen produced and heat input into the SOEC system per cubic meter of wastewater processed. For stream A, the electrolyzer enables the production of 26.2 kg of hydrogen per m³ of wastewater processed. In the case of stream C, with a lower vaporization rate, the hydrogen production decreases to 9.7 kg/m³. The electricity consumption for hydrogen production is 0.90 MWh/m³ for stream A and 0.33 MWh/m³ for stream C. The required thermal energy is lower, amounting to 0.38 MWh/m³ for stream A and 0.22 MWh/m³ for stream C. A significant portion of this thermal energy can be recovered by regenerating the exhaust gases from both the anode and the cathode, with 0.21 MWh/m³ and 0.14 MWh/m³ recovered for stream A and stream C, respectively. Stream C allows a higher recovery share (64%) compared to stream A (55%) due to its lower vaporization rate. Water evaporation represents the second most energy-intensive process in a plant, and the largest sub-stream (node 3 in Figure 2) that requires external energy supply.

Table 6. SOEC heat consumption and hydrogen production per m³ of wastewater stream processed (considering the two cases of stream A and stream C).

	Unit	STREAM A	STREAM C
Heat duty	[MWh/m ³]	0.38	0.22
Heat recovered	[MWh/m ³]	0.21	0.14
Heat from external sources	[MWh/m ³]	0.17	0.08
Heat share recovered	[%]	56	64
Electricity consumption	[MWh/m ³]	0.90	0.33
Wastewater vaporization	[%]	27	10
Clean water production	[L/m ³]	36.2	13.4
Hydrogen production	[kg/m ³]	26.2	9.7

In general, as shown in Table 7, the potential hydrogen production is 4067 tons per day for WWTP A and 268 tons per day for WWTP C. To achieve this, the power capacity required from the SOEC, considering a load factor of 50%, is 12.1 GW for stream A and 0.8 GW for stream C, respectively. As a byproduct, these plants could produce 5626 m³/d and 368 m³/d of fresh water.

Table 7. Key performance and assumptions of the SOEC system coupled with wastewater plants A and C on a daily basis.

	Unit	STREAM A	STREAM C
Wastewater flow rate	[m ³ /d]	155,347	27,500
SOEC load factor	[%]	50	50
SOEC power capacity	[GW]	12.1	0.8
Clean water production	[m ³ /d]	5626	368
Hydrogen production	[t/d]	4067	268

The production of hydrogen from WWTP A and WWTP C holds significant potential within the national energy landscape. In line with the European Union's energy transition program, Italy aims to install electrolyzers with a power capacity of 5 GW by 2030 [55]. Considering a maximum of 7500 h of operation per year (Best Scenario—BS) for an electrolyser with a moderate power of 2.12 V supported by wind and conventional energy, the estimated hydrogen production would be 0.10 Mt/y for WWTP C and 1.46 Mt/y for WWTP A. These figures correspond to approximately 15% (WWTP C) of and more than double (WWTP A) the national target. However, if the electrolyzer relies solely on wind energy, the operating time reduces to 2000 h per year (Worst Scenario—WS) [56]. In this

case, the hydrogen production decreases to 0.39 Mt/y for WWTP A and 0.03 Mt/y for WWTP C, while the contribution percentage to the national target remains the same.

Translating this hydrogen production into electricity contribution can be evaluated by considering that in 2030, Italy's national electricity demand is estimated to be around 366 TWh, with a renewable energy share of 75–84% [57]. This indicates that Italy needs to add between 8.6 and 10.7 GW of capacity per year to meet the growing demand. The solutions proposed in this article, utilizing wastewater from various WWTPs as sources of renewable energy, could contribute to meeting this pace.

In fact, if we consider that 850,000 tons of hydrogen can generate 43,000 GWh of electric power [58], the treated wastewater from WWTP A alone could cover 20% of the general electricity demand in the Best Scenario and 5.4% in the Worst Scenario. Similarly, the wastewater from the smaller WWTP C could cover 1.3% (BS) to 0.4% (WS) of the electricity need. These figures highlight the significant potential of utilizing wastewater as a renewable energy source and its contribution to meeting Italy's electricity requirements in a sustainable manner.

4. Conclusions

The urgent need to achieve “carbon neutrality” by 2050 has led the European Union to invest extensively in research focusing on clean energy solutions derived from renewable energy sources (RESs). In Italy, where the projected energy demand is estimated to reach 366 TWh by 2030, the EU target mandates that 75% to 84% of this demand must be met by RESs. Consequently, the search for environmentally sustainable approaches to electricity production is of paramount importance. Electrolysis of water for green hydrogen (H₂) production emerges as a promising option to consider.

In 2030, Italy's national electricity demand is estimated to be around 366 TWh, with a renewable energy share of 75–84% [57]. This indicates that Italy needs to add between 8.6 and 10.7 GW of capacity per year to meet the growing demand. The high share of renewable sources of electricity will require a storage capacity that, in EU countries, will reach 24% of electricity demand in 2030, where green H₂ is expected to play a major role [59]; moreover, the reshoring of high-hydrogen-demanding processes, such as ammonia and methanol production, will further increase the demand for green hydrogen and corresponding water consumption. The solutions proposed in this article, utilizing wastewater from various WWTPs as sources of renewable energy, could contribute to meeting this pace.

This study demonstrates that treated municipal wastewater obtained from wastewater treatment plants (WWTPs) of varying capacities, industrial loads, and treatment schemes can serve as an ideal water source for Solid Oxide Electrolysis Cells (SOECs) to produce “clean” hydrogen. Hydrogen generated through this process could contribute anywhere from 0.4% (worst-case scenario) to 20% (best-case scenario) of Italy's projected energy requirements for 2030. Moreover, when considering the widespread presence of WWTPs across regional or national territories, the potential contribution of wastewater-based hydrogen production becomes even more significant.

The primary objective of this study was to emphasize the possibility and energy viability of using impure water sources, specifically wastewater, for electrolytic green hydrogen production within the context of a circular economy. Future perspectives involve exploring the utilization of untreated wastewater as an input and examining whether this process could yield advantages from two perspectives: wastewater recovery, reuse, and in situ treatment, alongside hydrogen production for electricity generation.

If this approach proves to be valid, energy-efficient, and cost-effective, it could revolutionize the concept of clean energy production in regions where access to potable water is a challenge even for meeting basic needs. The symbiotic integration of wastewater treatment and hydrogen production has the potential to address multiple sustainability goals while simultaneously driving progress toward a decarbonized future. By capitalizing on these opportunities, countries not only can advance their renewable energy targets but also tackle water-related challenges, paving the way for a more sustainable and resilient future.

Author Contributions: Conceptualization, M.M. (Marina Maddaloni), N.A., and A.A.; Methodology, N.A., A.A., M.M. (Marina Maddaloni), M.M. (Matteo Marchionni), M.M. (Michele Mascia), and V.T.; validation, N.A., V.T. and M.M. (Michele Mascia); formal analysis, M.M. (Marina Maddaloni), N.A., M.M. (Michele Mascia), M.M. (Matteo Marchionni), A.A. and V.T.; investigation, M.M. (Marina Maddaloni), M.M. (Matteo Marchionni), and M.M. (Michele Mascia); resources, M.M. (Marina Maddaloni), M.M. (Matteo Marchionni), A.A. and G.B.; data curation, N.A., M.M. (Marina Maddaloni), A.A., M.M. (Matteo Marchionni), M.M. (Michele Mascia) and V.T.; writing—original draft preparation, M.M. (Marina Maddaloni), M.M. (Matteo Marchionni), and M.M. (Michele Mascia); writing—review and editing, N.A., V.T., M.P.C. and G.B.; visualization, N.A., V.T., M.P.C. and G.B.; supervision, N.A., V.T. and M.P.C.; project administration, N.A., V.T. and M.P.C.; funding acquisition, N.A., V.T. and M.P.C. All authors have read and agreed to the published version of the manuscript.

Funding: This research was funded by the European Union—NextGenerationEU—PROMETH2eus project-ID RSH2A_000039.

Data Availability Statement: All data generated or analysed during this study are included in this published article.

Conflicts of Interest: The authors declare no conflict of interest.

References

1. European Commission. *Communication from the Commission to the European Parliament, the Council, the European Economic and Social Committee and the Committee of The Regions—A European Strategy for Data*; European Commission: Brussels, Belgium, 2020.
2. Nagpal, D.; Abou Ali, A.; Feng, J.; Bianco, E.; Akande, D.; Escamilla, G.; Reiner, M.; Guinto, H.; Meattle, C.; Naran, B. Global Landscape of Renewable Energy Finance 2023. 2023. Available online: www.irena.org/publications (accessed on 2 May 2023).
3. Korberg, A.D.; Skov, I.R.; Mathiesen, B.V. The role of biogas and biogas-derived fuels in a 100% renewable energy system in Denmark. *Energy* **2020**, *199*, 117426. [[CrossRef](#)]
4. Mancò, G.; Guelpa, E.; Colangelo, A.; Virtuani, A.; Morbiato, T.; Verda, V. Innovative Renewable Technology Integration for Nearly Zero-Energy Buildings within the Re-cognition Project. *Sustainability* **2021**, *13*, 1938. [[CrossRef](#)]
5. Mohammadi, F.; Saif, M. A comprehensive overview of electric vehicle batteries market. *E-Prime-Adv. Electr. Eng. Electron. Energy* **2023**, *3*, 100127. [[CrossRef](#)]
6. Santos, G.; Smith, O. Electric vehicles and the energy generation mix in the UK: 2020–2050. *Energy Rep.* **2023**, *9*, 5612–5627. [[CrossRef](#)]
7. Pearre, N.S.; Kempton, W.; Guensler, R.L.; Elango, V.V. Electric vehicles: How much range is required for a day’s driving? *Transp. Res. Part C Emerg. Technol.* **2011**, *19*, 1171–1184. [[CrossRef](#)]
8. Wassiliadis, N.; Steinsträter, M.; Schreiber, M.; Rosner, P.; Nicoletti, L.; Schmid, F.; Ank, M.; Teichert, O.; Wildfeuer, L.; Schneider, J.; et al. Quantifying the state of the art of electric powertrains in battery electric vehicles: Range, efficiency, and lifetime from component to system level of the Volkswagen ID.3. *Etransportation* **2022**, *12*, 100167. [[CrossRef](#)]
9. Brynolf, S.; Hansson, J.; E Anderson, J.; Skov, I.R.; Wallington, T.J.; Grahm, M.; Korberg, A.D.; Malmgren, E.; Taljegård, M. Review of electrofuel feasibility—prospects for road, ocean, and air transport. *Prog. Energy* **2022**, *4*, 042007. [[CrossRef](#)]
10. Song, Z.; Liu, C. Energy efficient design and implementation of electric machines in air transport propulsion system. *Appl. Energy* **2022**, *322*, 119472. [[CrossRef](#)]
11. Pandit, K.; Jeffrey, C.; Keogh, J.; Tiwari, M.S.; Artioli, N.; Manyar, H.G. Techno-Economic Assessment and Sensitivity Analysis of Glycerol Valorization to Biofuel Additives via Esterification. *Ind. Eng. Chem. Res.* **2023**, *62*, 9201–9210. [[CrossRef](#)]
12. Salisu, J.; Gao, N.; Quan, C.; Yanik, J.; Artioli, N. Co-gasification of rice husk and plastic in the presence of CaO using a novel ANN model-incorporated Aspen plus simulation. *J. Energy Inst.* **2023**, *108*, 101239. [[CrossRef](#)]
13. Byrne, E.L.; O’donnell, R.; Gilmore, M.; Artioli, N.; Holbrey, J.D.; Swadźba-Kwaśny, M. Hydrophobic functional liquids based on trioctylphosphine oxide (TOPO) and carboxylic acids. *Phys. Chem. Chem. Phys.* **2020**, *22*, 24744–24763. [[CrossRef](#)] [[PubMed](#)]
14. O’donnell, R.; Ralphs, K.; Grolleau, M.; Manyar, H.; Artioli, N. Doping Manganese Oxides with Ceria and Ceria Zirconia Using a One-Pot Sol–Gel Method for Low Temperature Diesel Oxidation Catalysts. *Top. Catal.* **2020**, *63*, 351–362. [[CrossRef](#)]
15. Coney, C.; Hardacre, C.; Morgan, K.; Artioli, N.; York, A.P.; Millington, P.; Kolpin, A.; Goguet, A. Investigation of the oxygen storage capacity behaviour of three way catalysts using spatio-temporal analysis. *Appl. Catal. B Environ.* **2019**, *258*, 117918. [[CrossRef](#)]
16. Castoldi, L.; Matarrese, R.; Kubiak, L.; Daturi, M.; Artioli, N.; Pompa, S.; Lietti, L. In-depth insights into N₂O formation over Rh- and Pt-based LNT catalysts. *Catal. Today* **2019**, *320*, 141–151. [[CrossRef](#)]
17. Leonzio, G.; Zondervan, E.; Foscolo, P.U. Methanol production by CO₂ hydrogenation: Analysis and simulation of reactor performance. *Int. J. Hydrog. Energy* **2019**, *44*, 7915–7933. [[CrossRef](#)]
18. Kirsten, K.; Hadler, J.; Schmidt, P.; Weindorf, W. Alternative Fuels in the Well-to-Wheel Debate. *ATZextra Worldw.* **2016**, *21*, 38–43. [[CrossRef](#)]

19. Ullah, A.; Hashim, N.A.; Rabuni, M.F.; Junaidi, M.U.M. A Review on Methanol as a Clean Energy Carrier: Roles of Zeolite in Improving Production Efficiency. *Energies* **2023**, *16*, 1482. [[CrossRef](#)]
20. Ulucan, T.H.; Akhade, S.; Ambalakatte, A.; Autrey, T.; Cairns, A.; Chen, P.; Cho, Y.W.; Gallucci, F.; Gao, W.; Grinderslev, J.B.; et al. Hydrogen storage in liquid hydrogen carriers: Recent activities and new trends. *Prog. Energy* **2023**, *5*, 12004. [[CrossRef](#)]
21. Xie, S.; Li, Z.; Li, H.; Fang, Y. Integration of carbon capture with heterogeneous catalysis toward methanol production: Chemistry, challenges, and opportunities. *Catal. Rev.* **2023**, *5*, 1–40. [[CrossRef](#)]
22. Chen, C.; Yang, A. Power-to-methanol: The role of process flexibility in the integration of variable renewable energy into chemical production. *Energy Convers. Manag.* **2021**, *228*, 113673. [[CrossRef](#)]
23. Bos, M.J.; Kersten, S.R.A.; Brilman, D.W.F. Wind power to methanol: Renewable methanol production using electricity, electrolysis of water and CO₂ air capture. *Appl. Energy* **2020**, *264*, 114672. [[CrossRef](#)]
24. Shi, X.; Liao, X.; Li, Y. Quantification of fresh water consumption and scarcity footprints of hydrogen from water electrolysis: A methodology framework. *Renew. Energy* **2020**, *154*, 786–796. [[CrossRef](#)]
25. Vermeiren, P.; Adriansens, W.; Moreels, J.; Leysen, R. Evaluation of the Zirfon[®] separator for use in alkaline water electrolysis and Ni-H₂ batteries. *Int. J. Hydrog. Energy* **1998**, *23*, 321–324. [[CrossRef](#)]
26. Palmas, S.; Rodriguez, J.; Mais, L.; Mascia, M.; Herrando, M.C.; Vacca, A. Anion exchange membrane: A valuable perspective in emerging technologies of low temperature water electrolysis. *Curr. Opin. Electrochem.* **2023**, *37*, 101178. [[CrossRef](#)]
27. Kumar, S.S.; Himabindu, V. Hydrogen production by PEM water electrolysis—A review. *Mater. Sci. Energy Technol.* **2019**, *2*, 442–454. [[CrossRef](#)]
28. Rotraut, M. *High-Temperature Electrolysis*; IOP Publishing: Bristol, UK, 2023. [[CrossRef](#)]
29. Hauch, A.; Küngas, R.; Blennow, P.; Hansen, A.B.; Mathiesen, B.V.; Mogensen, M.B. Recent advances in solid oxide cell technology for electrolysis. *Science* **2020**, *370*, 6513. [[CrossRef](#)] [[PubMed](#)]
30. Gómez, S.Y.; Hotza, D. Current developments in reversible solid oxide fuel cells. *Renew. Sustain. Energy Rev.* **2016**, *61*, 155–174. [[CrossRef](#)]
31. Zhang, L.; Hu, S.; Zhu, X.; Yang, W. Electrochemical reduction of CO₂ in solid oxide electrolysis cells. *J. Energy Chem.* **2017**, *26*, 593–601. [[CrossRef](#)]
32. Laguna-Bercero, M.A. Recent advances in high temperature electrolysis using solid oxide fuel cells: A review. *J. Power Sources* **2012**, *203*, 4–16. [[CrossRef](#)]
33. Peng, J.; Huang, J.; Wu, X.-L.; Xu, Y.-W.; Chen, H.; Li, X. Solid oxide fuel cell (SOFC) performance evaluation, fault diagnosis and health control: A review. *J. Power Sources* **2021**, *505*, 230058. [[CrossRef](#)]
34. IPCC. *Global Warming of 1.5 °C*; Cambridge University Press: Cambridge, UK, 2022. [[CrossRef](#)]
35. Simoes, S.G.; Catarino, J.; Picado, A.; Lopes, T.F.; di Bernardino, S.; Amorim, F.; Gírio, F.; Rangel, C.; de Leão, T.P. Water availability and water usage solutions for electrolysis in hydrogen production. *J. Clean. Prod.* **2021**, *315*, 128124. [[CrossRef](#)]
36. Xu, W.; Scott, K. The effects of ionomer content on PEM water electrolyser membrane electrode assembly performance. *Int. J. Hydrog. Energy* **2010**, *35*, 12029–12037. [[CrossRef](#)]
37. Lim, C.K.; Liu, Q.; Zhou, J.; Sun, Q.; Chan, S.H. High-temperature electrolysis of synthetic seawater using solid oxide electrolyzer cells. *J. Power Sources* **2017**, *342*, 79–87. [[CrossRef](#)]
38. Liu, Z.; Han, B.; Lu, Z.; Guan, W.; Li, Y.; Song, C.; Chen, L.; Singhal, S.C. Efficiency and stability of hydrogen production from seawater using solid oxide electrolysis cells. *Appl. Energy* **2021**, *300*, 117439. [[CrossRef](#)]
39. Meier, K. Hydrogen production with sea water electrolysis using Norwegian offshore wind energy potentials: Techno-economic assessment for an offshore-based hydrogen production approach with state-of-the-art technology. *Int. J. Energy Environ. Eng.* **2014**, *5*, 1–12. [[CrossRef](#)]
40. Khan, M.A.; Al-Attas, T.; Roy, S.; Rahman, M.M.; Ghaffour, N.; Thangadurai, V.; Larter, S.; Hu, J.; Ajayan, P.M.; Kibria, G. Seawater electrolysis for hydrogen production: A solution looking for a problem? *Energy Environ. Sci.* **2021**, *14*, 4831–4839. [[CrossRef](#)]
41. Quan, C.; Zhang, G.; Gao, N.; Su, S.; Artioli, N.; Feng, D. Behavior Study of Migration and Transformation of Heavy Metals during Oily Sludge Pyrolysis. *Energy Fuels* **2022**, *36*, 8311–8322. [[CrossRef](#)]
42. Sikosana, M.L.; Sikhwivhilu, K.; Moutloali, R.; Madyira, D.M. Municipal wastewater treatment technologies: A review. *Procedia Manuf.* **2019**, *35*, 1018–1024. [[CrossRef](#)]
43. Chan, Y.J.; Chong, M.F.; Law, C.L.; Hassell, D. A review on anaerobic–aerobic treatment of industrial and municipal wastewater. *Chem. Eng. J.* **2009**, *155*, 1–18. [[CrossRef](#)]
44. Al-Malah, K.I. *Aspen Plus—Chemical Engineering Applications*; Aspen Plus[®], John Wiley & Sons, Inc.: Hoboken, NJ, USA, 2016; pp. i–xxxi. [[CrossRef](#)]
45. Ni, M.; Leung, M.K.H.; Leung, D.Y.C. An Electrochemical Model of a Solid Oxide Steam Electrolyzer for Hydrogen Production. *Chem. Eng. Technol.* **2006**, *29*, 636–642. [[CrossRef](#)]
46. Ni, M.; Leung, M.K.; Leung, D.Y. Parametric study of solid oxide fuel cell performance. *Energy Convers. Manag.* **2007**, *48*, 1525–1535. [[CrossRef](#)]
47. Ni, M.; Leung, M.K.; Leung, D.Y. Parametric study of solid oxide steam electrolyzer for hydrogen production. *Int. J. Hydrog. Energy* **2007**, *32*, 2305–2313. [[CrossRef](#)]
48. Noren, D.; Hoffman, M. Clarifying the Butler–Volmer equation and related approximations for calculating activation losses in solid oxide fuel cell models. *J. Power Sources* **2005**, *152*, 175–181. [[CrossRef](#)]

49. EG&G Technical Services Inc. *Fuel Cell Handbook*, 7th ed.; U.S. Department of Energy Office of Fossil Energy: Morgantown, West Virginia, 2004.
50. Lonis, F.; Tola, V.; Cau, G. Renewable methanol production and use through reversible solid oxide cells and recycled CO₂ hydrogenation. *Fuel* **2019**, *246*, 500–515. [CrossRef]
51. Gazzetta Ufficiale Della Repubblica Italiana, Government of Italy Legislative Decree 3 April 2006, n. 152. Environmental Regulations. Available online: <https://www.gazzettaufficiale.it/dettaglio/codici/materiaAmbientale> (accessed on 2 May 2023). (In Italian).
52. Regione Lombardia, Lombardy Regional Regulation 29 March 2019, n. 6. Regulation and Administrative Regimes for Domestic Wastewater and Urban Wastewater Discharges, Regulation of Discharge Controls and Methods for Approving Projects for Urban Wastewater Treatment Plants, in, 2019. Available online: https://normelombardia.consiglio.regione.lombardia.it/NormeLombardia/Accessibile/main.aspx?view=showdoc&iddoc=rr002019032900006&exp_coll=rr002019032900006&selnode=rr002019032900006 (accessed on 5 July 2023). (In Italian).
53. Momma, A.; Kato, T.; Kaga, Y.; Nagata, S. Polarization Behavior of High Temperature Solid Oxide Electrolysis Cells (SOEC). *J. Ceram. Soc. Jpn.* **1997**, *105*, 369–373. [CrossRef]
54. Petipas, F.; Brisse, A.; Bouallou, C. Thermal management of solid oxide electrolysis cell systems through air flow regulation. *Chem. Eng. Trans.* **2017**, *61*, 1069–1074. [CrossRef]
55. Di, D.F.; Setti, L. Study on Green Hydrogen Economic Sustainability for an Italian Hydrogen Backbone. 2022, pp. 1–40. Available online: <https://www.qualenergia.it/wp-content/uploads/2022/07/Studio-idrogeno-ReCommon.pdf> (accessed on 5 July 2023). (In Italian).
56. Arnal, J.; Tecnalìa, M.I. H2aeolus-Environmental Performance Analysis, 7 March 2023. Available online: <https://www.haeolus.eu/?p=1177> (accessed on 5 July 2023).
57. Politecnico di Milano, Renewable Energy Report 2023-Italian. 2023. Available online: <https://www.energystrategy.it/es-download/> (accessed on 5 July 2023). (In Italian).
58. Ministero Dello Sviluppo Economico, Strategia Nazionale Idrogeno–Linee Guida Preliminari, (2020) 21. Available online: https://www.mise.gov.it/images/stories/documenti/Strategia_Nazionale_Idrogeno_Linee_guida_preliminari_nov20.pdf (accessed on 5 July 2023).
59. European Commission. Recommendations on Energy Storage. 2023. Available online: https://energy.ec.europa.eu/topics/research-and-technology/energy-storage/recommendations-energy-storage_en (accessed on 5 July 2023).

Disclaimer/Publisher’s Note: The statements, opinions and data contained in all publications are solely those of the individual author(s) and contributor(s) and not of MDPI and/or the editor(s). MDPI and/or the editor(s) disclaim responsibility for any injury to people or property resulting from any ideas, methods, instructions or products referred to in the content.